Nomenclature

Quantities listed without units are dimensionless.

Roman Symbols

a	phase interfacial area per unit volume of flow (m^2/m^3 or 1/m)
A_{col}	cross-sectional area of bubble column (m^2)
C, C_n	arbitrary constant or parameter
C_D	drag coefficient
D_b	bubble diameter (m)
D_{col}	diameter of bubble column (m)
D_{cyl}	diameter of cylindrical test object (cm)
D_L	mass diffusion coefficient into liquid phase (m^2/s)
D_{Sauter}	Sauter mean bubble diameter (m)
$\mathbf{D}$	tomographic measurement domain
E	Maxwell-Hewitt conductivity function
f	frequency (Hz)
f_b	bubble size distribution function
f_{large}	fraction of gas volume in bimodal bubble size distribution attributed to large bubbles
$f_{\max}$	value of f_{large} at which monodisperse and bimodal Maxwell-Hewitt relations differ most
f_μ	gamma attenuation distribution function
F_n	weight function for fundamental voltage at electrode n
g	gravitational constant, 9.807 m/s^2
H_{col}	height of multiphase mixture in bubble column (m)
I	injected current (A)
j_G	gas volumetric flux density ($m^3/s/m^2$ or m/s)
$\bar{j}_G$	alternative notation for superficial gas velocity ($m^3/s/m^2$ or m/s)
j_{Gd}	gas volumetric drift flux ($m^3/s/m^2$ or m/s)
j_L	liquid volumetric flux density ($m^3/s/m^2$ or m/s)
j_{Ld}	liquid volumetric drift flux ($m^3/s/m^2$ or m/s)
j_m	mixture volumetric flux density ($m^3/s/m^2$ or m/s)

J	injected current per unit length of electrode (A/m)
k	fitted coefficient
k_L	mass transfer coefficient into liquid phase (m/s)
K	fixed parameter
l_P	Prandtl mixing length scale (m)
L	distance above floor of bubble column (cm)
M	number of possible independent measurements at the tomographic domain boundary, also number of impedance elements in the computed domain reconstruction
M_G	gas phase momentum per unit mass (kg·m/s/kg or m/s)
$\mathbf{n}$	unit normal vector outward from the domain boundary
N	number of electrodes on the domain boundary
p_{col}	fluid pressure in two-phase bubble column flow (Pa or kPa)
p_v	vapor pressure of liquid at ambient temperature (Pa or kPa)
q	charge flux on the domain boundary (A/m^2)
Q_G	gas volumetric flow rate (m^3/s)
r	radial coordinate (m)
$\tilde{r}$	normalized radial coordinate
R_b	radius of bubble, drop, or particle (m)
R_b^*	nondimensionalized radius of bubble, drop, or particle
R_{col}	radius of bubble column or EIT testbed (m)
Sh	Sherwood number, $k_L D_b / D_L$
T_L	liquid temperature (ºC or K)
T_G	gas temperature (ºC or K)
u_b	bubble rise velocity (m/s)
$u_{b\infty}$	terminal velocity of a single bubble, drop, or particle (m/s)
u_{Dd}	dispersed phase drift velocity (m/s)
u_G	gas phase velocity (m/s)
$\overline{u}_G$	column-averaged gas phase velocity (m/s)
u_{Gd}	gas phase drift velocity (m/s)
u_L	liquid phase velocity (m/s)
u_{Ld}	liquid phase drift velocity (m/s)
u_r	relative velocity or slip velocity (m/s)
$\langle u_r \rangle$	relative velocity averaged over the flow cross section (m/s)
U_G	superficial gas velocity, equal to gas volumetric flux density averaged over the flow cross section ($m^3/s/m^2$ or m/s)

$U_{G,trans}$ superficial gas velocity at regime transition ($m^3/s/m^2$ or m/s)

U_m superficial mixture velocity, equal to mixture volumetric flux density averaged over the flow cross section ($m^3/s/m^2$ or m/s)

V voltage or electric potential (V)

$\overline{V}$ voltage averaged over the measurement period (V)

V_{col} volume of fluid in bubble column (m^3)

V_n fundamental voltage solution at electrode n

$V_n^{(ij)}$ fundamental voltage solution at electrode n for injection at electrode i and withdrawal at electrode j

$\tilde{V}_m^{(ij)}$ measured voltage at electrode m for injection electrode i and withdrawal electrode j (V)

$\hat{V}_m^{(ij)}$ weighted voltage "measurement" for injection electrode i, withdrawal electrode j, and measurement electrode m

w distance from center of insulating test object (m)

$w_m^{(ij)}$ fundamental voltage weight for injection electrode i, withdrawal electrode j, and measurement electrode m

x Cartesian coordinate in bubble column or domain (m)

y Cartesian coordinate in bubble column or domain (m)

z Cartesian or cylindrical axial coordinate (m)

Greek Symbols

α Maxwell-Hewitt coefficient

β momentum correction factor

γ complex electrical conductivity (S/m or μS/cm)

δ_{qr} Kronecker delta function

$\overline{\varepsilon}_{cyl}$ volume fraction of testbed occupied by test object

ε_D volume fraction of dispersed phase

$\varepsilon_{D,MAX}$ volume fraction of dispersed phase at maximum packing

ε_{df} "dense phase" volume fraction of small bubbles in a liquid-small bubble mixture, excluding volume of large bubbles

$\overline{\varepsilon}_{df}$ dense phase holdup, column-averaged volume fraction of small bubbles in a liquid-small bubble mixture excluding volume of large bubbles

ε_G gas volume fraction

$\langle \varepsilon_G \rangle$ gas volume fraction averaged across the column cross section

$\overline{\varepsilon}_G$ gas holdup or volume-averaged gas volume fraction

$\varepsilon_{G,small}$ volume fraction of small bubbles in two-phase flow

$\varepsilon_{G,large}$	volume fraction of large bubbles in two-phase flow
$\bar{\varepsilon}_{G,small}$	column-averaged volume fraction of small bubbles
$\bar{\varepsilon}_{G,large}$	column-averaged volume fraction of large bubbles
$\bar{\varepsilon}_{G,trans}$	gas holdup at regime transition
ε_I	insulating phase volume fraction
ε_L	liquid volume fraction
$\bar{\varepsilon}_L$	volume-averaged liquid volume fraction
ε_S	solid volume fraction
$\langle \varepsilon_S \rangle$	solid volume fraction averaged across the column cross section
$\bar{\varepsilon}_S$	volume-averaged solid volume fraction
$\bar{\varepsilon}_S^{NOM}$	nominal column-averaged solid volume fraction
η_C	dynamic viscosity of continuous phase (kg/m/s)
η_D	dynamic viscosity of dispersed phase (kg/m/s)
η_{eff}	effective dynamic viscosity of non-Newtonian fluid (kg/m/s)
η_L	liquid dynamic viscosity (kg/m/s)
η_m	mixture dynamic viscosity (kg/m/s)
θ	azimuthal coordinate (degrees)
μ	gamma ray attenuation coefficient (1/cm)
$\hat{\mu}$	gamma ray attenuation coefficient averaged over the beam path (1/cm)
$\langle \mu \rangle$	gamma ray attenuation coefficient averaged over the measurement cross section (1/cm)
μ_G	gas phase gamma ray attenuation coefficient (1/cm)
μ_L	liquid phase gamma ray attenuation coefficient (1/cm)
μ_S	solid phase gamma ray attenuation coefficient (1/cm)
ν_L	liquid kinematic viscosity (m^2/s)
ν_{mol}	molecular kinematic viscosity (m^2/s)
ν_t	turbulent eddy viscosity (m^2/s)
ξ	variable in the Maxwell-Hewitt conductivity function
ρ	density (kg/m^3)
ρ_C	density of continuous phase (kg/m^3)
ρ_D	density of dispersed phase (kg/m^3)
ρ_G	gas density (kg/m^3)
ρ_L	liquid density (kg/m^3)

ρ_S	solid density (kg/m^3)
σ	real component of complex electrical conductivity (S/m or μS/cm)
$\overline{\sigma}$	effective or domain-averaged real conductivity (S/m or μS/cm)
σ_B	effective conductivity of mixture of liquid and bimodal (small and large) bubbles (S/m or μS/cm)
σ_{df}	effective conductivity of "dense phase" mixture of liquid and small bubbles, excluding large bubbles (S/m or μS/cm)
σ_L	real electrical conductivity of liquid phase (S/m or μS/cm)
σ_s	interfacial surface tension (N/m)
τ_{rz}	shear stress in the radial direction on a plane perpendicular to the vertical axis (kg/m/s^2)
ω	permittivity or dielectric constant (F/m or μF/cm)
$\tilde{\omega}$	permittivity of medium relative to vacuum
$\tilde{\omega}_L$	relative permittivity of liquid
ω_0	permittivity of vacuum, 8.854×10^{-12} F/m

Quantitative Tomographic Measurements of Opaque Multiphase Flows

1. Introduction

The spatial distribution of materials in dispersed multiphase flows is important to many chemical and energy industries. For example, bubble-column reactors are used to carry out chemical synthesis and other processes in gas-liquid or gas-solid-liquid flows; in indirect coal liquefaction, a reactive gas is bubbled through a catalyst-laden slurry. When scaling slurry bubble-column reactor vessels to industrial sizes, it is important to ensure that the distribution of the different materials within the vessel is acceptable. A spatially nonuniform gas distribution within the reactor can reduce process efficiency by inducing large-scale, buoyancy-driven recirculating flows (Jackson *et al.*, 1996). Thus, it is desirable to be able to accurately measure or predict material distributions in three-phase flows.

Because direct numerical simulation of multiphase flows based on first principles is presently impractical, computational models for industrial use must rely on a combination of theory and experimental correlations to properly simulate such flows. Techniques that measure the distribution of each phase in multiphase flows have the potential to improve the control of such processes and can also be useful for validating computational models (Plaskowski *et al.*, 1995; Torczynski *et al.*, 1997). As the requirements for accuracy of computational models become more demanding, the techniques used to measure relevant flow properties must deliver more detailed and accurate information.

A dilemma encountered in multiphase flow measurements is that probes or instruments should be placed outside the flow domain so as not to disturb the flow itself, but phase distributions cannot easily be measured from the boundary. Tomography offers a possible solution to this dilemma, since tomographic methods have the potential to determine spatial phase distributions without disturbing the flow. Many of the tomographic instruments available to study multiphase flows have been derived from devices for medical applications. Examples of these methods include X-ray tomography; nuclear magnetic resonance (NMR, also known as magnetic resonance imaging or MRI); positron emission tomography (PET); and acoustic tomography. While the spatial resolution of these methods can be substantial (acoustic tomography can have a resolution of less than 1 mm, MRI a resolution of 10^{-5} m), these methods are often limited to the study of slowly changing systems because of the long acquisition times required for accurate quantitative data (ranging from minutes for MRI to hours for PET and other

radiation-based methods). The systems listed above can also be difficult to use because of safety and cost considerations. In recent years the medical community has pioneered the use of electrical-impedance tomography (EIT), which uses measurements of the electrical impedance at the boundary of a test domain to reconstruct the impedance within the domain. EIT has the potential for much faster quantitative measurements of phase distributions than other tomographic methods. Researchers are now attempting to implement EIT systems for the nonintrusive study of multiphase flows. Dickin *et al.* (1993) and Ceccio and George (1996) report on the development of EIT systems specifically for multiphase flows, while a review of current developments in many of the other fields of tomography can be found in George *et al.* (1998a).

At Sandia National Laboratories, initial research into multiphase tomographic methods was performed as part of the Laboratory-Directed Research and Development (LDRD) project "Advanced Tomographic Flow Diagnostics for Opaque Multiphase Fluids." The final report for this LDRD (Torczynski *et al.*, 1997) examined several techniques for measuring phase distributions in vertical bubble-column flows, including instruments that provided spatially averaged or local quantities and other methods designed to yield full-field, spatially resolved measurements. Two tomographic techniques, gamma-densitometry tomography (GDT) and electrical-impedance tomography (EIT), were applied to two-phase flows and compared to established measurement methods and to one another. The EIT system was developed as a joint effort between Sandia National Laboratories and the University of Michigan (O'Hern *et al.*, 1995; Torczynski *et al.*, 1996a).

GDT and other radiation-based tomographic methods are relatively mature and are known to measure spatial phase distributions accurately (Hewitt, 1978). Shollenberger *et al.* (1997a) applied the GDT technique at Sandia to vertical gas-liquid flows at industrially relevant conditions and reported that GDT accurately measured the phase distributions (see also Torczynski *et al.*, 1997). The main disadvantage of radiation-based methods, as suggested above, is that the data collection times required are usually longer than the time scales of time-dependent multiphase flows. EIT can acquire information much more quickly than GDT, but several issues with EIT are currently under investigation, including its usefulness for multiphase flows, its spatial resolution, and its ability to make accurate quantitative measurements (Webster, 1990; Jones *et al.*, 1993; Plaskowski *et al.*, 1995; Ceccio and George, 1996). While Torczynski *et al.* (1997) were able to report successful EIT measurements only of a dilute solid-liquid suspension, subsequent improvements to data acquisition and reduction yielded the first validated, quantitative phase distribution measurements with EIT (George *et al.*, 1998a).

This report documents the work conducted since the publication of the LDRD report, specifically the application of the EIT and GDT techniques to the task of providing spatially resolved information on dispersed multiphase flows. Torczynski *et al.* (1997) briefly discussed the complexity of multiphase fluid mechanics as a motivation for this work; Chapter 2 of this report expands upon this topic by summarizing recent investigations into the physics of vertical bubble-column flows. Subsequent chapters discuss the application of GDT and EIT at Sandia to two-phase and three-phase vertical column flows. Chapter 3 includes a brief introduction to EIT theory and a description of the Sandia/Michigan EIT system. Recent improvements to the EIT hardware are described, and numerical and experimental validation tests of the EIT reconstruction algorithm are presented. The EIT system is then evaluated in Chapter 4 for its

ability to measure realistic solid-liquid and gas-liquid flows. Since the Sandia GDT system had already been successfully applied to multiphase flows (Adkins *et al.*, 1996; Torczynski *et al.*, 1996b; Shollenberger *et al.*, 1997a), it was used to assess the accuracy of the EIT system in two-phase flow measurements. Finally, a three-phase tomographic method combining GDT and EIT is presented in Chapter 5 and applied to several vertical solid-gas-liquid flows to provide information useful for the design and scaleup of bubble-column reactors. Typically, EIT systems have been validated by imaging static conductivity distributions or (in a few cases) by quantifying small-scale two-phase flows. This study marks a significant application of EIT to quantitative measurements of multiphase flows on a scale approaching that of bubble-column reactors and other industrial flows.

2. A Review of Vertical Multiphase Flow Studies

This report discusses the application of tomographic techniques to vertical multiphase flows, which are flows of considerable importance to the chemical and nuclear industries. For example, bubble-column reactors are commonly used in the chemical industry to carry out fermentation, extraction, or coal liquefaction. These reactors are essentially vertical columns in which gas enters from the bottom and bubbles through a continuous liquid phase or solid-liquid slurry. The ability to predict the phase distributions, rate of mass transfer, and chemical reaction rates in these columns is a key to improving performance, but scaling the hydrodynamic and transport behavior from the laboratory to industrial conditions remains a formidable task. In the nuclear power industry, boiling is used as a highly efficient heat transfer mechanism in a class of reactors known as boiling water reactors (BWRs). Here the working fluid undergoes nucleate boiling and exhibits a range of flow regimes along the vertical coolant channels in the core. The local vapor phase distribution influences fuel heat transfer characteristics and core reactivity. Improved understanding of the vertical two-phase flows in BWRs under normal and abnormal conditions is currently leading to increases in reactor efficiency, simplified designs, and improved safety.

This chapter reviews the literature on the vertical flows found in two-phase and three-phase chemical reactors, particularly bubble-column reactors. It is in this area that electrical-impedance tomography (EIT) is currently being applied at Sandia to try to obtain information for bubble-column reactor design. This review begins with a discussion of the variables relevant to describing and predicting vertical multiphase flows and flows in bubble-column reactors. Experimental data and correlations from the literature are presented, then models of vertical flows are reviewed. The chapter ends with a survey of current methods of scaling the relevant parameters from the laboratory setting to industrial conditions. Successful scaling is the key to much-needed improvements in the design of bubble-column reactors and similar facilities.

2.1. Relevant Quantities in Vertical Multiphase Flows

The first task in modeling a process for predictive purposes is to determine the variables that must be measured and correctly scaled between laboratory and prototype conditions. Beyond the obvious choices of fluid properties and variables of state — density, temperature, pressure, surface tension, and so on — hydrodynamic variables and phase spatial distributions must be examined to characterize multiphase flows correctly. One of the first journal articles to present a method for analyzing and interpreting experimental data from two-phase flow systems was that of Zuber and Findlay (1965). Many physical quantities were defined or cited in that reference that have become standard for describing multiphase flows. The definitions, introduced below, assume a gas-liquid flow with motion along only one axis, although the equations are equally applicable to other two-phase flows with motion in one dimension.

The first useful quantity is the volumetric flux density, j_ϕ, defined as the volume flow rate of phase ϕ per unit area of the column or duct perpendicular to the direction of flow. The volumetric flux density of each phase is defined in terms of the local phase volume fraction, ε_ϕ, and the local phase velocity, u_ϕ.

$$j_G = \varepsilon_G u_G \tag{2.1}$$

$$j_L = (1-\varepsilon_G)u_L = \varepsilon_L u_L \tag{2.2}$$

The volumetric flux density of the mixture is defined as the sum of the local values for each phase, so that in gas-liquid flow

$$j_m = j_L + j_G . \tag{2.3}$$

Another useful quantity is the drift velocity, $u_{\phi d}$. This is defined as the phase velocity with respect to the mixture volumetric flux density, and may also be thought of as the phase velocity relative to a hypothetical surface moving with the average velocity of the mixture at the location of interest.

$$u_{Gd} = u_G - j_m \tag{2.4}$$

$$u_{Ld} = u_L - j_m \tag{2.5}$$

Similarly, the volumetric drift flux is defined as the volumetric flux density of the phase relative to the hypothetical surface (Wallis, 1969; Shah and Deckwer, 1983).

$$j_{Gd} = \varepsilon_G u_{Gd} = (1-\varepsilon_G) j_G - \varepsilon_G j_L \tag{2.6}$$

$$j_{Ld} = \varepsilon_L u_{Ld} = (1-\varepsilon_L) j_L - \varepsilon_L j_G = -j_{Gd} \tag{2.7}$$

Finally, the difference in u_G and the local velocity of the liquid phase, u_L, is referred to as the relative velocity or "slip velocity" (Shah and Deckwer, 1983):

$$u_r = u_G - u_L = \frac{j_G}{\varepsilon_G} - \frac{j_L}{1-\varepsilon_G} . \tag{2.8}$$

By convention the relative velocity is the velocity of the gas relative to the liquid; u_G and u_L have the same sign if the one-dimensional motions of the two phases are in the same direction. If there is no flow of the liquid phase in or out of the bubble column, the reactor is said to be operating in "batch mode," and consequently, $j_L = u_L = 0$ and $u_r = u_G$. Many investigators have found the relative velocity to be a strong influence on gas-liquid flows.

In many cases, local quantities such as volumetric flux density and drift flux cannot be measured directly, but the experimenter can easily obtain values averaged over the area of the column or flow duct. For example, the area-averaged gas volumetric flux density can be computed directly from the gas volumetric flow rate, Q_G, and the area of the flow:

$$U_G = \bar{j}_G \equiv \frac{1}{A_{col}} \int_A j_G dA_{col} = \frac{Q_G}{A_{col}}. \tag{2.9}$$

This particular average is commonly called the "superficial gas velocity." (By convention, superficial velocities of phase ϕ are denoted by U_ϕ rather than $\bar{j}_\phi$.) Similarly, the column-averaged gas volume fraction, $\bar{\varepsilon}_G$, has historically been called "gas holdup" because it can be determined from the rise in the free surface of the fluid mixture with gas flow in the column:

$$\bar{\varepsilon}_G \equiv \frac{1}{V_{col}} \int_V \varepsilon_G dV_{col} = \frac{\Delta H_{col}}{H_{col} + \Delta H_{col}}. \tag{2.10}$$

(In this chapter, $\bar{\varepsilon}_G$ will be referred to as "gas holdup" because of the prevalence of the term in the literature; however, "average gas volume fraction" is the more accurate description.) Early works almost exclusively report correlations and measurements of average quantities, such as U_ϕ and $\bar{\varepsilon}_\phi$, whereas local values – *e.g.*, radial phase distributions – have been reported in the literature only recently with the advent of particle imaging velocimetry and tomographic techniques.

2.2. Experimental Data and Correlations

This section discusses investigations of flow patterns, gas volume fractions, and mass transfer parameters in vertical bubble columns. Particular attention is paid to operating conditions and phase properties that influence the flows, as this is important in the scaleup of laboratory results to industrial conditions. Most of the experimental data taken in vertical column flows involves gas-liquid flows; although slurry bubble-column reactors and fluidized bed reactors involve a solid phase, little data has been reported for such systems.

The flow regimes of vertical gas-liquid flows are well known and have been correlated for a wide range of flow parameters (Shah and Deckwer, 1983; Carey, 1992). Examples of the flow regimes relevant to bubble-column hydrodynamics are sketched in Figure 2.1. At low superficial gas velocities, the bubbles are roughly uniform in diameter and are much smaller than the column itself. The bubbles are dispersed rather evenly in the liquid phase, rise at about the same velocity, and rarely interact with one another. This flow regime is known as "homogeneous bubbly flow" or simply "bubbly flow." At higher superficial gas velocities, larger bubbles form, the flow becomes heterogeneous, and the behavior of the phases depends upon the size of the column. In larger columns of the size found in industrial applications, small and large bubbles coexist, and the larger bubbles rise at higher velocities, generating turbulent

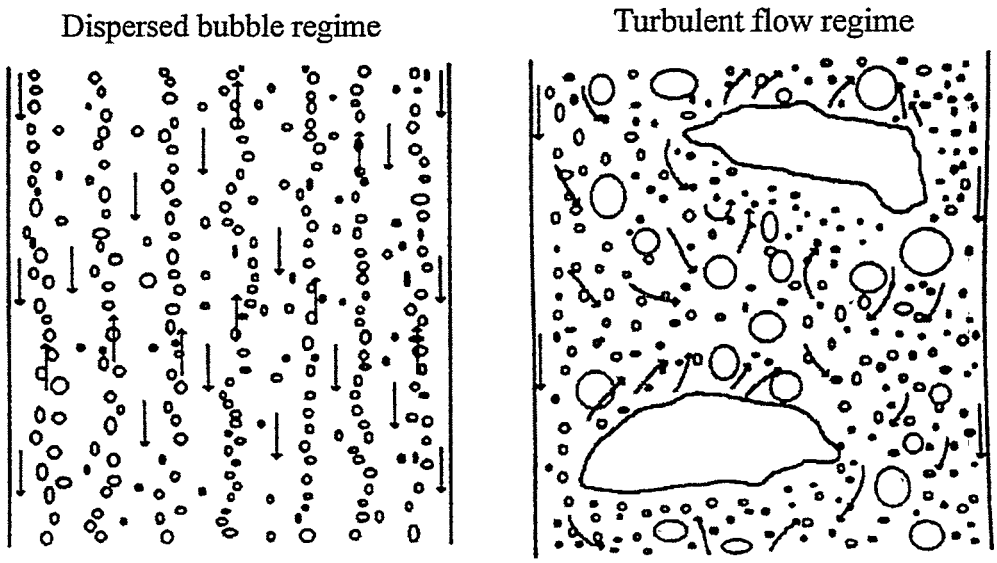

Figure 2.1. Vertical gas-liquid flow regimes of interest in bubble-column hydrodynamics. (Left) homogeneous bubbly flow, (right) churn-turbulent flow. All arrows denote the direction of liquid motion. Adapted from Chen *et al.* (1994).

motion in the liquid phase. This flow is known as "churn-turbulent" flow. In small-diameter vertical columns – typically columns with internal diameters less than 15 cm – the walls act to prevent churn-turbulent flow and cause the gas phase to coalesce into slugs with diameters comparable to the column itself. This may occur in columns with diameters larger than 15 cm if the liquid phase is sufficiently viscous, but "slug flow" is not typically found in bubble-column reactors and is therefore not of concern here.

The flow regime map for air-water bubble columns (Figure 2.2), which indicates the regime as a function of column diameter and superficial gas velocity, is typical of general gas-liquid flows. Many of the investigations reviewed in this chapter are concerned with the transition between gas-liquid flow regimes or with the lower limit on column diameter for which churn-turbulent flows occur.

2.2.1. Gas Volume Fraction Correlations and Observations

Most of the experimental data taken in vertical column flows is of gas volume fractions in gas-liquid flows. This is due not only to the wide variety of methods available for measuring ε_G, but also because of the influence of this quantity on chemical reaction rates and liquid recirculation in bubble-column reactors.

One of the first comprehensive studies of gas volume fraction in bubble columns was that of Akita and Yoshida (1973), in which the rise in liquid level during gas flow was measured and translated into gas holdup for 24 different combinations of liquids, gases, liquid temperature, and column diameter. The paper presented a correlation based on dimensional analysis that fit the

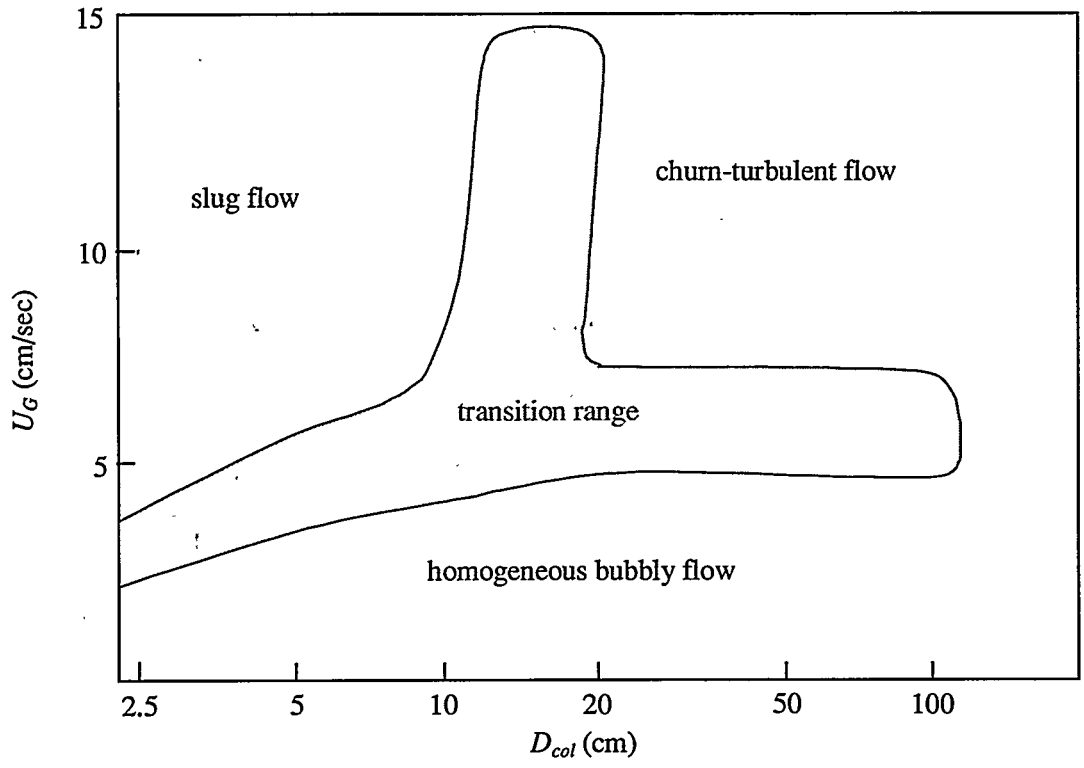

Figure 2.2. Flow regime map for vertical air-water bubble columns (adapted from Shah and Deckwer, 1983).

gas holdup in bubbly flow well. The dimensional analysis included surface tension, σ_s, the superficial gas velocity, U_G, and the column diameter, D_{col}, as independent variables and yielded the correlation

$$\frac{\bar{\varepsilon}_G}{(1-\bar{\varepsilon}_G)^4} = C\left(\frac{gD_{col}^2\rho_L}{\sigma_s}\right)^{1/8}\left(\frac{gD_{col}^3}{\nu_L^2}\right)^{1/12}\frac{U_G}{\sqrt{gD_{col}}}, \tag{2.11}$$

where $C = 0.20$ for pure liquids and nonelectrolyte solutions and 0.25 for electrolyte solutions. According to the authors, earlier experiments had shown the effect of the column diameter on gas holdup to be negligible for columns with diameters of 15 cm or larger. Only columns meeting this criterion were used in their experiments, and their final correlation was chosen to reflect the independence of $\bar{\varepsilon}_G$ on column diameter (note that D_{col} cancels on the right-hand side of Eq. 2.11). Deckwer and Schumpe (1993) advocate a similar correlation for gas flows in viscous liquids and non-Newtonian fluids,

$$\bar{\varepsilon}_G = 0.20\left(\frac{gD_{col}^2\rho_L}{\sigma_s}\right)^{-0.13}\left(\frac{gD_{col}^3\rho_L^2}{\eta_{eff}^2}\right)^{0.11}\left(\frac{U_G}{\sqrt{gD_{col}}}\right)^{0.54}, \tag{2.12}$$

where the liquid kinematic viscosity in Eq. 2.11 has been replaced by the ratio of the effective dynamic viscosity to the liquid density, η_{eff}/ρ_L, to account for non-Newtonian behavior. Note also that this correlation does show a dependence on column diameter ($\bar{\varepsilon}_G \propto D_{col}^{-0.20}$).

The independence of $\bar{\varepsilon}_G$ from D_{col} observed by Akita and Yoshida has been confirmed by later researchers (Shah *et al.*, 1982; Wilkinson *et al.*, 1992; Kumar *et al.*, 1994, 1997) and is the result of the absence of slug flow in industrially relevant liquids when $D_{col} \geq 15$ cm. This value is generally accepted as the lower limit for scaleup of experimental results to industrial scales, provided the following conditions are met: (1) the experimental flow is in the churn-turbulent regime, and (2) the experimental liquid column has a height-to-diameter ratio such that $(H_{col}/D_{col}) \geq 5$ (Joshi *et al.*, 1998). As the first condition suggests, flows in highly viscous or non-Newtonian liquids will have a different lower scaleup limit on D_{col}.

Influences on gas volume fraction with flow rate have been studied extensively, possibly because gas volumetric flow rate is the easiest variable to modify in bubble-column experiments. The relationship between gas holdup and superficial gas velocity is known to vary with flow regime. It is generally accepted as a characteristic of the bubbly flow regime that $\bar{\varepsilon}_G$ increases linearly with U_G (Wilkinson *et al.*, 1992; Reilly *et al.*, 1994). In the churn-turbulent regime the relationship is generally believed to take the form $\bar{\varepsilon}_G \propto U_G^n$, where $n < 1$. Reported values of n range from 0.4 to 0.8 (Wilkinson *et al.*, 1992; Shah *et al.*, 1982). In churn-turbulent flows observed by Reilly *et al.* (1994), the relationship between $\bar{\varepsilon}_G$ and U_G was linear in a few gas-liquid systems, but the slope was consistently less steep than in the bubbly flow regime.

Wilkinson *et al.* (1992) experimentally investigated the effects of column dimensions on $\bar{\varepsilon}_G$ and other quantities to assist in the scaleup of laboratory results to industrial conditions. Measurements were made of nitrogen holdup by an overflow method in four liquids, with surface tensions differing by a factor of 3, viscosities varying by a factor of 50, and fluid pressures ranging from atmospheric to 2.0 MPa. The group confirmed earlier findings that gas holdup decreases with increasing column diameter until $D_{col} > 15$ cm, beyond which the diameter has no effect. For columns with liquid height-to-diameter ratios such that $3 < (H_{col}/D_{col}) < 5$, increasing the column height was found to induce stronger liquid circulation, thereby reducing gas volume fraction gradients between the central column region, the sparger or entrance region, and any foamy region present at the free surface. The net result of an increase in H_{col} over this range was to decrease $\bar{\varepsilon}_G$ within the column. For columns with absolute height $H_{col} > 3$ m or columns with $(H_{col}/D_{col}) > 5$, the influence of circulation and end effects became negligible. Ueyama and Miyauchi (1979) found D_{col} to have little influence on the functional relationship between $\bar{\varepsilon}_G$ and U_G, both in their gas holdup model and in experimental data with which the model was compared; notably, some of the data came from experiments with $D_{col} = 13.8$ cm, less than the commonly accepted limit of 15 cm below which slug flow occurs.

Wilkinson (1991) investigated the influence of sparger hole size on gas holdup. In tests with different gases and liquids, sparger holes had no effect on $\bar{\varepsilon}_G$, provided that the hole diameter was larger than 2 mm. Joshi *et al.* (1998) reported a similar critical hole diameter for several experiments in churn-turbulent air-water flows and flows involving an aqueous solution of carboxymethyl cellulose. Below their critical hole diameter of 3 mm, however, $\bar{\varepsilon}_G$ increased as hole diameter decreased.

The properties of the liquid and gas phases are also relevant quantities that can be easily varied experimentally, and whose effects have yet to be understood fully for correct scaleup of column behavior. A review by Wilkinson (1991) found that with all other conditions being equal, column-averaged gas volume fractions increase with gas density (see also Deckwer and Schumpe, 1993; Krishna and Ellenberger, 1996). Increases in ρ_G increase bubble instability and breakup, which reduces the typical bubble diameter, D_b; decreases the terminal velocity of the bubbles, $u_{b\infty}$; and causes an increase in gas holdup through continuity (see Eq. 2.1). Reilly *et al.* (1994) measured the effects of gas density on gas holdup using a differential pressure method, using gases ranging from helium (ρ_G = 0.164 kg/m^3) to CO_2 (ρ_G = 1.84 kg/m^3) and liquids ranging from trichloroethylene ($\eta_L = 5.75\times10^{-4}$ kg/m/s) to a viscous petroleum hydrocarbon ($\eta_L = 2.43\times10^{-3}$ kg/m/s). Increases in the overall column pressure from atmospheric to p_{col} = 1.1 MPa were also used in experiments to increase gas density. The gas volume fraction in both bubbly and churn-turbulent flow regimes was deduced to be a function of the gas phase momentum, M_G, which incorporates the influences of both gas density and gas velocity. The following power law relationship was determined for both bubbly and churn-turbulent flows:

$$\bar{\varepsilon}_G = C_0 \beta^n \left[\frac{\rho_G U_G}{(1-\bar{\varepsilon}_G)\rho_L} \right]^n = C_1 M_G^n . \qquad (2.13)$$

The exponent n and the constants C_0 and C_1 ($\equiv C_0\beta^n$) all depend upon flow regime, and the units of the constants are defined so as to render the correlation nondimensional. The parameter β is a correction factor that accounts for differences between the column-averaged axial gas phase velocity, $\bar{u}_G$, and the local values of u_G, which can include radial or azimuthal components.

Log-log plots of $\bar{\varepsilon}_G$ versus M_G justified this power-law correlation under experimental conditions and indicated appropriate values of n. In the bubbly flow regime, n = 1, and the constant C_1 is determined by the gas density. Data from churn-turbulent flows of all gas-liquid systems investigated fell on a line described by n = 1/3. One assumption in the derivation of Eq. 2.13 was found to fail under high-pressure "pilot plant" conditions: at high gas holdups ($\bar{\varepsilon}_G$ > 0.5), the total mass of the gas phase relative to that of the liquid phase is no longer negligible, invalidating the approximation for M_G. Reilly and co-workers discuss how the gas momentum term must be evaluated based on the masses of both phases to extend the applicability of the power law to higher gas pressures.

Concerning liquid properties, the only properties determined by Reilly *et al.* (1994) to significantly influence gas holdup in ambient two-phase flows were ρ_L (included in Eq. 2.13) and surface tension, σ_s. From a variety of gases bubbled through trichloroethylene, water, and industrial hydrocarbons, Reilly and co-workers found the effect to be described best by the relationship $\bar{\varepsilon}_G(1-\bar{\varepsilon}_G) \propto \sigma_s^{-0.12}$ or $C_1 \propto \sigma_s^{-0.12}$ in bubbly flows. The effect on churn-turbulent flows was smaller and was not quantified. Wilkinson *et al.* (1992) reviewed the work of earlier authors and found that results often depend on the method used to vary liquid properties. They did point out, however, that factors that lower the bubble coalescence rate will increase gas holdup through reduction of bubble size.

Of particular importance to the scaleup of laboratory results to operating conditions is the effect of temperature and pressure on phase properties. Zou *et al.* (1988) reported measurements of gas holdup in air-liquid co-current column flows at elevated operating temperatures representative of industrial conditions. Data were taken in air-alcohol, air-saline, and air-water systems, and a single correlation for $\bar{\varepsilon}_G$ in the three systems was obtained using dimensional analysis and the experimental data. The dimensional analysis is noteworthy for the inclusion of the vapor pressure of the liquid phase, p_v, which was significantly different at the higher liquid temperatures than at ambient conditions.

The data indicated a strong dependence of gas volume fraction upon liquid temperature; with increasing T_L, the air bubbles became smaller, and $\bar{\varepsilon}_G$ increased in a nearly second-order fashion. While no explanation for decreasing bubble size was advanced by the authors, decreases in η_L and σ_s with increasing T_L are likely candidates, as these encourage smaller bubbles and bubble breakup. Air-alcohol flows were found to have higher gas holdups for the same volumetric flow rates and conditions; because of the higher vapor pressure of alcohol relative to water, higher amounts of vapor were collected by the air bubbles during their rise toward the free surface. The addition of NaCl to the water phase also produced a higher value of $\bar{\varepsilon}_G$, and the change could be accounted for by a temperature-dependent correction. The increase in gas holdup with the addition of electrolyte is attributed to a lower coalescence rate of the gas phase. Though the exact mechanism involved is not discussed, the decrease of surface tension with the added electrolyte is the most probable cause. Finally, it was noted that earlier correlations of $\bar{\varepsilon}_G$, including that of Hughmark (1967) for the bubbly flow regime, failed at elevated temperatures because the correlations assumed constant values of fluid properties.

Lin *et al.* (1998) published an informative work on scaleup of bubble-column phenomena in which bubble-scale and column-scale phenomena were studied for dependence upon both operating temperatures and pressures. Single-bubble rise velocities, u_b; bubble coalescence and breakup; and gas holdup, $\bar{\varepsilon}_G$, were observed for nitrogen gas in a column of Paratherm NF (a heat transfer fluid) at system pressures up to 20 MPa and liquid temperatures from T_L = 27°C to 78°C. Bubble rise velocities were distinctly affected by changes in physical properties of both phases with pressure and temperature. From the Paratherm-N_2 data, u_b was found to decrease with increases in fluid pressure, the prevalent cause being the resultant decrease in the density difference $\Delta\rho = \rho_L - \rho_G$ and its effect on the buoyancy force. An extensive discussion of the

effects of pressure and temperature on bubble formation, coalescence, and breakup can also be found in the paper. In summary, the distribution of the bubble diameter, D_b, shifted toward smaller diameters with an increase in fluid pressure (as the resulting increases in ρ_G and gas momentum encouraged the formation of smaller bubbles), while changes in temperature of the system resulted in competing effects on D_b. Both u_b and D_b, of course, influence the gas holdup.

Similar observations of pressure and bubble velocity were made by Adkins *et al.* (1996) in air-water flows at elevated pressure. A review of experimental data in the literature (Joshi *et al.*, 1998) finds that, depending upon flow conditions and bubble shape, drag forces on an individual bubble are proportional to D_b^m, where m ranges from 1 (for spherical bubbles in low Reynolds number flows) to 3.25 (for ellipsoidal bubbles at high Reynolds numbers in contaminated liquids). As argued by Adkins *et al.* (1996), since buoyancy forces scale as D_b^3, a force balance would determine that bubble velocity is proportional to D_b^{3-m}, and almost never inversely proportional to bubble diameter. The decrease in both D_b and u_b with increasing pressure is therefore to be expected.

In general, $\bar{\varepsilon}_G$ was found by Lin *et al.* (1998) to increase with rising system temperature in agreement with Zou *et al.* (1988). The precise influence of T_L and T_G on $\bar{\varepsilon}_G$ is complex, depending on the interaction between η_L, ρ_G, and σ_s, which can be unique to each multiphase system. The gas holdup was also found to increase with rising fluid pressure, which may be rationalized by the corresponding decreases in u_b and D_b described above. These pressure effects were more pronounced at higher gas volumetric fluxes, all else being equal. The end result of variations in both pressure and temperature on $\bar{\varepsilon}_G$ may be thought of as an imbalance between viscosity on one hand and gas momentum and surface tension on the other.

The last topic of this section is the behavior of local values of gas volume fraction, as opposed to average gas holdup. While the investigations described to this point consider only the column-averaged gas volume fraction, tomographic methods are available to measure time-averaged spatial profiles of ε_G. Kumar *et al.* (1997) used gamma-ray computed tomography to measure gas volume fractions in two-dimensional cross sections of air-water vertical column flows. The distributions were nearly axisymmetric and were circumferentially averaged over θ to produce distributions in r alone. In general, their results were described well by the customary power law (see, for example, Ueyama and Miyauchi, 1979),

$$\varepsilon_G(r) = C_\varepsilon \frac{n+2}{n}\left[1 - C_w\left(\frac{r}{R_{col}}\right)^n\right], \tag{2.14}$$

where C_ε is a parameter related to $\bar{\varepsilon}_G$, C_w accounts for the nonzero gas volume fraction at the wall, and the exponent n quantifies the "steepness" of the profile. For the larger columns used in tests, a value of n between 2 and 2.5 was in best agreement with the data. Gas volume fractions

averaged over the measurement cross section (area averages) were also computed from the data and compared to gas holdup values (volume averages) from differential pressure measurements and bed expansion measurements to validate the tomographic approach.

Effects of several operating parameters on $\varepsilon_G(r)$ were reported. In both bubbly and churn-turbulent flow, the gas distributions were influenced by D_{col}, with profiles becoming more peaked with increasing column diameter over the range 10 cm $\leq D_{col} \leq$ 30 cm. However, the area-averaged gas volume fraction, $\langle \varepsilon_G \rangle$, is in line with the accepted trend of the volume-averaged gas volume fraction, $\bar{\varepsilon}_G$, of remaining unchanged with diameter, provided that $D_{col} >$ 15 cm. In general, an increase in U_G led to an increase in $\varepsilon_G(r)$ everywhere except near the wall, making the parabolic profile steeper; this effect was more pronounced in bubbly flows. Additional experiments with a water-isopropanol mixture as the liquid phase revealed that the increase in $\varepsilon_G(r)$ with decreasing surface tension extended all the way out to the column walls because the smaller gas bubbles that result are able to migrate closer to the periphery of the flow.

Adkins *et al.* (1996) also used gamma-ray tomography to determine the radial distribution of air in an industrial-scale bubble column and to investigate the effects of pressure on the gas phase distribution. The bubble column was a stainless steel pressure vessel with D_{col} = 48 cm, considerably larger than the lower scaleup limit of 15 cm. Air-water vertical flows at fluid pressures from 177 kPa to 432 kPa were analyzed for trends in $\bar{\varepsilon}_G$ and $\varepsilon_G(r)$. The profiles were similar to those of Kumar *et al.* (1997): highest at the column axis, parabolic in shape, and increasing more at the axis than at the walls as U_G increased. For a given superficial velocity, however, the gas volume fraction profile was found to increase uniformly across the column as fluid pressure was increased. Later studies in the same bubble column with air and Drakeol 10 (a light mineral oil) exhibited the same trends in $\varepsilon_G(r)$ with pressure (Torczynski *et al.*, 1997).

2.2.2. Mass Transfer Correlations

Bubble-column reactors exist to synthesize an end product, usually through chemical reactions. Mass transfer rates between phases have also been measured under laboratory conditions in the hope of translating results to full-scale conditions. The rate of mass transfer to phase ϕ from another phase is expressed as the product of a mass transfer coefficient, k_ϕ, and the interfacial area between phases per unit volume, a. The product $k_L a$ is usually referred to as a volumetric coefficient for mass transfer to the liquid phase, and has units of reciprocal seconds. For correlations, k_ϕ is often combined with the mass diffusion coefficient, D_ϕ, and a relevant length scale to form a Sherwood number, Sh. For example, mass transfer from a gas bubble of diameter D_b to a surrounding continuous liquid phase can be described by the quantity

$$Sh \equiv \frac{k_L D_b}{D_L}. \tag{2.15}$$

The dimensionless group $(k_L a D_b^2 / D_L)$ is also commonly used.

An early paper by Hughmark (1967) proposed a semi-theoretical correlation for the liquid phase mass transfer coefficient in bubble columns, based on published data for air and a variety of liquids in the bubbly flow regime. The correlation agreed with the published data to within about 20%. Akita and Yoshida (1973) postulated another correlation for *Sh* based on dimensional analysis and experiments with oxygen bubbled through various liquids. To determine the mass transfer coefficient empirically, liquid samples were analyzed chemically for oxygen content after each test. While the correlation was in fair agreement with the data, the authors recommended "due caution" in its use with other systems. An improvement by Öztürk *et al.* (1987) on this correlation determined from a variety of gas-liquid systems is in better agreement with experimental data (average error 13%) and accounts for changes in gas density:

$$\left(\frac{k_L a D_b^2}{D_L}\right) = 0.62\left(\frac{\nu_L}{D_L}\right)^{0.5}\left(\frac{g\rho_L D_b^2}{\sigma_s}\right)^{0.33}\left(\frac{g D_b^3}{\nu_L^2}\right)^{0.29}\left(\frac{U_G}{\sqrt{g D_b}}\right)^{0.68}\left(\frac{\rho_G}{\rho_L}\right)^{0.04}. \qquad (2.16)$$

Another study of mass transfer was made by Wilkinson *et al.* (1994). In this set of experiments, air was bubbled through a sodium sulfite solution, and the oxidation rate of the sodium sulfite was measured. The goal was to find the influence of fluid pressure on bubble sizes and mass transfer coefficients. Both $\bar{\varepsilon}_G$ and the volumetric mass transfer coefficient, $k_L a$, were found in experiments to increase significantly with increasing pressure of the phases, especially at high superficial gas velocities. Given the observation in the previous section that the average bubble size decreases as the pressure in the column rises, the trend in mass transfer with pressure is to be expected, since the interfacial area density, a, and the gas holdup are related by

$$a = \frac{6\bar{\varepsilon}_G}{D_{Sauter}}. \qquad (2.17)$$

The Sauter mean bubble diameter, D_{Sauter}, is defined as the diameter of a hypothetical bubble having the same volume per unit surface area as the average of all bubbles in the flow. If the bubble size distribution in the flow of interest is $f_b(D_b)$, then the Sauter mean bubble diameter may be expressed as (Fan and Zhu, 1998)

$$D_{Sauter} \equiv \frac{\int_0^\infty D_b^3 f_b(D_b) dD_b}{\int_0^\infty D_b^2 f_b(D_b) dD_b}. \qquad (2.18)$$

The trend in $k_L a$ with pressure observed by Wilkinson and co-workers was reversed at fluid pressures approaching 1.5 MPa when a foamy structure formed in the sodium sulfite solution. This foam decreased the local liquid volume fraction, limited the amount of sulfite in solution available to be oxidized, and decreased the mass transfer rate. Other variables found to improve

the mass transfer coefficient included superficial gas velocity (higher U_G led to turbulence and to bubble breakup) and the addition of electrolytes such as sodium sulfite (which reduced the coalescence rate).

Based on a limited set of data from this study, Wilkinson *et al.* (1994) proposed an empirical correlation for D_{Sauter} that accounted for fluid pressure and its effect on gas density.

$$\frac{g\rho_L D_{Sauter}^2}{\sigma_s} = 8.8\left(\frac{U_G\eta_L}{\sigma_s}\right)^{-0.04}\left(\frac{\sigma_s^3\rho_L}{g\eta_L^4}\right)^{-0.12}\left(\frac{\rho_L}{\rho_G}\right)^{0.22} \tag{2.19}$$

For the mass transfer coefficient itself, they tentatively suggested the following relationship between two cases in which the same gas is introduced at different conditions.

$$\frac{[(k_L a)\rho_G]_2}{[(k_L a)\rho_G]_1} = \left\{\frac{[(\bar{\varepsilon}_G)\rho_G]_2}{[(\bar{\varepsilon}_G)\rho_G]_1}\right\}^n \tag{2.20}$$

Here n is estimated to range from 1.0 to 1.2. It was noted that validation of the general relationship requires data from other liquids and further research of the influences of ρ_G and p_{col} on $\bar{\varepsilon}_G$ and $k_L a$.

2.2.3. Flow Regime Transitions

Because of the increased mixing in turbulent flows, a useful parameter in bubble-column design is the transition point from bubbly flow to churn-turbulence in gas-liquid vertical flows, or the transition point to an analogous regime in gas-solid or three-phase flows. Wilkinson *et al.* (1992) discuss influences on the transition from homogeneous to churn-turbulent flow in gas-liquid vertical flows. Through empirical correlations they determined that the superficial gas velocity at transition $U_{G,trans}$ and the gas holdup at transition $\bar{\varepsilon}_{G,trans}$ increase under the following circumstances: (1) with the addition of electrolytes to the liquid phase (which reduces bubble coalescence), (2) with increases in gas density (because of the increase in bubble breakup), and (3) with decreases in η_L and σ_s (which reduce initial bubble size). From regression analysis, they obtained the following empirical equation for $\bar{\varepsilon}_{G,trans}$:

$$\bar{\varepsilon}_{G,trans} = 0.5 \cdot \exp(-193\rho_G^{-0.61}\eta_L^{0.5}\sigma_s^{0.11}). \tag{2.21}$$

Valid ranges of the phase properties are: $\sigma_s = 0.02 - 0.073$ N/m, $\eta_L = 0.0004 - 0.055$ kg/m/s, $\rho_G = 0.09 - 3.8$ kg/m^3. The typical error of this correlation was just under 10% of the experimental value of $\bar{\varepsilon}_{G,trans}$. By comparison, Reilly *et al.* (1994) used their power-law relationship (Eq. 2.13) to derive the transition formulas